Asian Journal of Chemistry; Vol. 35, No. 6 (2023), 1341-1346

ASIAN JOURNAL OF CHEMISTRY

https://doi.org/10.14233/ajchem.2023.27796

Effects of Axial Ligands on the Redox Properties of Manganese(III) *meso-tetrakis*(*p*-Hydroxyphenyl) Porphyrin

V. THANDIAYYAKONE[1], A. MURUGAN[2,*], C.R. RAVIKUMAR[3], T. RAJKUMAR[4], A. KULANDAISAMY[5], IJAZ ULLAH MUZADDADI[2], A. MANOHAR[6], P. THILLAI ARASU[7] and MITHUN CHAKRABARTY[8]

[1]Research and Development Centre, Bharathiar University, Coimbatore-641046, India
[2]Department of Chemistry, North Eastern Regional Institute of Science & Technology, Nirjuli, Itanagar-791109, India
[3]Department of Chemistry, East West Institute of Technology, Bangalore-560091, India
[4]Department of Chemistry, Rajah Serfoji Government College (Affiliated to Bharathidasan University), Thanjavur-613005, India
[5]Department of Chemistry, Government Arts and Science College, Sivakasi-626124, India
[6]Department of Chemistry, Periyar Maniammai Institute of Science and Technology, Periyar Nagar, Vallam, Thanjavur-613403, India
[7]Department of Chemistry, College of Natural and Computational Science, Wollega University, Wollega, Ethiopia
[8]Department of Chemistry, St. Anthony's College, Shillong-793001, India

*Corresponding author: E-mail: nspmmurugan@gmail.com

Received: 15 March 2023; *Accepted*: 11 April 2023; *Published online*: 27 May 2023; AJC-21248

In this work, *meso-tetrakis*(*p*-Hydroxyphenyl) porphyrin [T(*p*-OH)PP] and manganese(III) *meso-tetrakis*(*p*-hydroxyphenyl) porphyrin Mn[T(*p*-OH)PP] were synthesized and characterized. The UV-visible and cyclic voltammetry were used to evaluate the axial ligand and redox behaviour of Mn[T(*p*-OH)PP]. The addition of ethylamine, diethylamine and *tertiary* amines to Mn(III) *meso*-porphyrins distinguishes their axial ligand characteristics. The presence of ethylamine causes the octahedral geometry to transform into a square pyramidal structure. Cyclic voltammetry shows that Mn(III) converts to Mn(II) porphyrins. Additionally, the UV-visible spectrophotometry and cyclic voltammetry were also used to investigate the oxidation process.

Keywords: Manganese, *meso*-Porphyrin, Axial effect, Electrochemical properties.

INTRODUCTION

The liver of fish, birds and vertebrates contain porphyrins, many of which are connected to the electron transport of the respiratory chain [1]. Cytochrome P-450 enzymes are found in bacterial chlorophyll and are used to catalyze a variety of reactions. Enzymes that include porphyrin also participate in oxidative reactions, either directly or by an indirect process involving a reaction with hydrogen peroxide [1]. It has been demonstrated that iron porphyrin (TPPBrx)FeCl (TPPBrx) is the dianion of β-brominated-pyrrole tetraphenylporphyrin and x = 0-8) is subject to quasi-reversible one-electron oxidations as a result of the conjugated porphyrin ring structure. Two competing effects of the interaction of CO with metalloporphyrin are the propensity of the bromine substituents to remove electrons and the non-planarity of the macrocycle [2].

Axial ligands properties of ruthenium porphyrin have been shifted to longer wavelengths due to the addition of tetrabutylammonium hydroxide. Ruthenium porphyrin has shown two reversible oxidation and one irreversible reduction, which is used to characterize the one electron-transfer reactions [3]. *meso*-Substituted porphyrins have shown the formation of dianion radical due to inclined by the electron donor properties of the porphyrin substituents using tetrabutylammonium hexafluorophosphate as supporting electrolyte and their corresponding diffusion coefficients have been calculated [4]. New ferrocene-functionalized porphyrins and ruthenocene-functionalized porphyrin have exhibited reversible one-electron transfers because the porphyrin ligand has little effect on the ferrocene [5]. Due to the electrical interaction between the porphyrin ring and the peripheral ruthenium complexes *via* the pyridyl bridges, ruthenium porphyrin has generated a peak at

693 nm. The coordination of phenanthroline to the peripheral ruthenium sites boosted the intermolecular force *e.g*. van der Waals that were formed, which in turn raised the stability of the films in an aqueous solution and improved the response time of the modified electrodes to reduce analytes like dopamine. Ru(III) has been transformed to Ru(II) porphyrin, according to electrochemical investigations, which involved the mono-electronic reductions involving the porphyrin ring [6].

Due to the structural deformation in the porphyrin system and associated electrical connection of aluminium porphyrin to the salicylate intermediated by the Al^{3+} ion, aluminium(III)-*p*-methyl-*meso*-tetraphenylporphyrin has displayed a little red shift. Because the signals of the axial ligand protons are shifted to a higher field than the signals of the porphyrin protons, salicylate groups axially ligated to Al(III) porphyrins to create five-coordinate complexes of Al(III) porphyrins. Reversible redox potentials were present in aluminium(III)-porphyrin [7]. The isoporphyrin's electrochemical study revealed one irreversible reduction at a relatively low potential and these findings supported the theory that reducing agents can effectively reduce metalloporphyrins [8].

The manganese(III) *meso* porphyrins' absorption spectra exhibit three Soret bands, which served as a guide for the octahedral geometry showed synthesis of manganese(III). The octahedral geometry of Mn^{3+} state is transformed to a tetragonal complexes with the addition of secondary amines as a result of the creation of 5th and 6th axial coordination at in-plane Mn porphyrin. This Mn(III) porphyrin can be converted into square pyramidal manganese(II) porphyrin, which has the typical visible spectrum of Mn(II) porphyrin, using primary amine and *p*-anion radicals. In Mn(III) *meso* porphyrin, Mn is in a high spin d^4 form with octahedral geometry. The shape of Mn(II) porphyrin changes to square pyramidal Mn(II) porphyrin when ethylamine is introduced. In square pyramidal Mn(II) porphyrin, the Mn atom is in a high-spin d^5 configuration with the occupied $d_{x^2-y^2}$ orbital, which has a low orbital energy and Mn(III) will consequently be outside the porphyrin plane [9]. When diethylamine was added after a weak back bond, the geometry of Mn(III) porphyrins changed to a tetragonal complex. Tetragonal complex creation appears to reduce bonding. This may happen as a result of the in-plane metal porphyrin expanding and absorbing two of the ethylamine's axial ligands. The geometry modifications demonstrated that the two ethyl amine groups occupy the 5th and 6th positions as axial coordination sites due to the availability of two ethylamine from ethyl, diethyl and triethyl amines. The presence of fluorine in the phenyl rings of porphyrins as well as the location of their positive charges on the N-methyl pyridinium group have a significant impact on how they interact with DNA [10]. Literature-based evaluations were done on manganese(III) *meso*-5, 10, 15 and 20-*tetrakis*(*p*-hydroxyphenyl)porphyrin Mn[T(*p*-OH)PP] (Fig. 1). Complexes have been produced and their axial ligand and redox properties have been evaluated using cyclic voltammetry and UV-visible spectrophotometry.

EXPERIMENTAL

Synthesis: *meso*-5,10,15,20-*tetrakis*(*p*-hydroxyphenyl) porphyrin [T(*p*-OH)PP] and tetra-*n*-butylammonium iodide were bought from Aldrich and utilized without additional purification. Prior to usage, dichloromethane was distilled after being refluxed over phosphorous pentoxide. Manganese(III) *meso*-*tetrakis*(*p*-hydroxyphenyl)porphyrin, Mn[T(*p*-OH)PP] has been synthesized [9]. Tetra-*n*-butylammonium perchlorate (TBAP) was prepared by reacting tetra-*n*-butylammonium iodide with sodium perchlorate and then recrystallized from methanol.

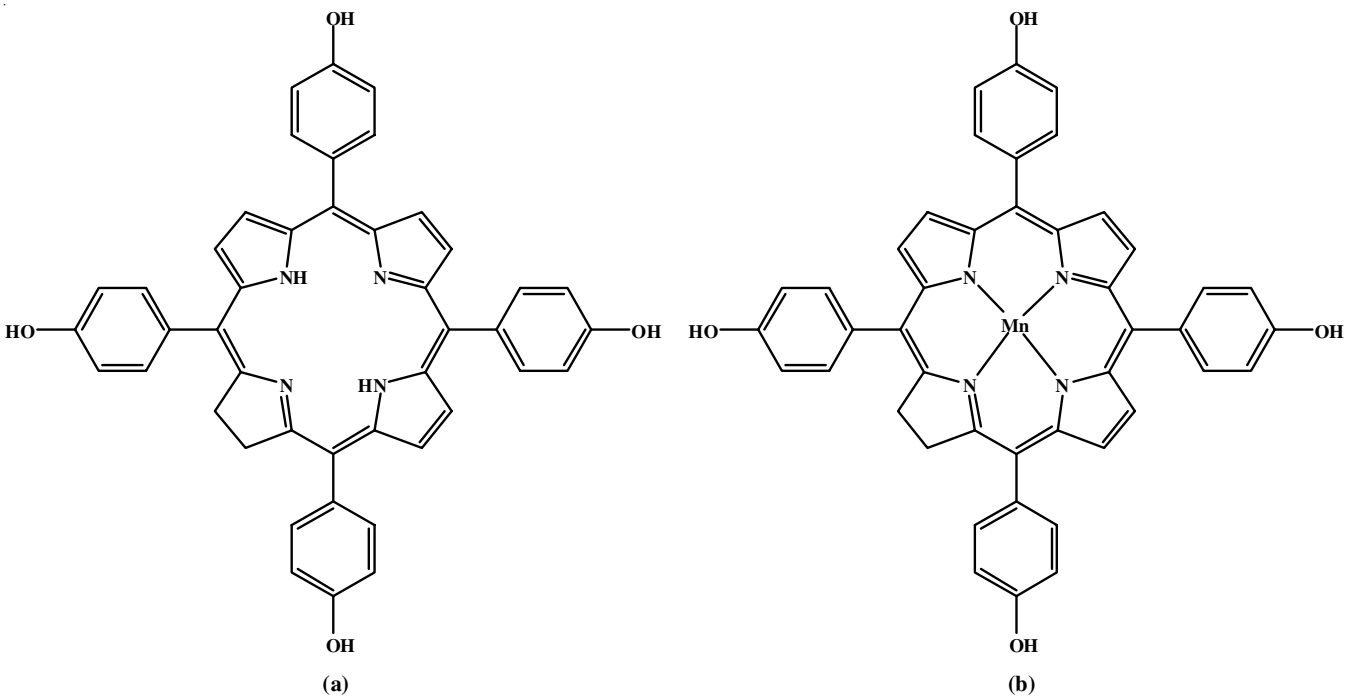

Fig. 1. Structure of *meso*-5, 10, 15, 20-*Tetrakis*(*p*-hydroxyphenyl)porphyrin, [T(*p*-OH)PP] (a) and manganese *meso*-5, 10, 15, 20-*tetrakis*(*p*-hydroxyphenyl)porphyrin, Mn[T(*p*-OH)PP] (b)

The cyclic voltammetric measurements and UV-visible spectrophotometer measurement were performed [11]. The visible spectra were measured in the 300-750 nm region. The reduction properties of individual 0.05 mM 1º, 2º and 3º-amines were evaluated in a quartz cuvette.

RESULTS AND DISCUSSION

Cyclic voltammetric studies of Mn[T(*p*-OH)PP]: Mn[T(*p*-OH)PP] has three different oxidation potentials of 0.7500, 0.9280 and 1.1632 volts and three different reduction potentials of 0.5360, 0.7810 and 1.1424 volts. The values of ΔE were 0.2170, 0.1490 and 0.0212 volts (Fig. 2a). The $E_{1/2}$ values were 0.8545, 1.1528 and 0.6430 volts. In Mn[T(*p*-OH)-PP, the first and second ligand oxidations take place at 0.9280V and 1.1632V, respectively and about 0.7500V, manganese transitions from Mn(III) to Mn(IV). Because of changes in geometry at the structure of manganese porphyrin complex, the hydroxy group is an electron-donating group and the oxidation potentials must be shifted higher [12-15]. A monocation or dication radical may arise, according to the 1.1632 V oxidation value. In the macrocycle compound the electron density is increased by the electron-donor hydroxy group (-OH). As a result, after oxidation potential reductions, the removal of electrons becomes simpler. In order to make the equivalent monomeric species easier to reduce and harder to oxidize, the energy of the HOMO and LUMO as well as the electron density of the π-ring system would have been reduced by the electron-donating hydroxyl group [16]. Since, it is necessary for the creation of Mn(IV) porphyrin ring system, the higher oxidation state of Mn(IV) ion indicates a stabilizing effect [17]. The ratio of anodic to cathodic peak current (I_{pc}/I_{pa}) is equal to one because of the one-electron reversible transfer that takes place. Due to the quasi-reversible process, the first and second porphyrin ligand oxidations demonstrate that i_{pc}/i_{pa} is greater than one [18]. The production of Mn(II) ions is shown in **Scheme-I**.

Fig. 2b does not resolve the cyclic voltammetric spectra of reduction potentials, while Fig. 2b displays the measured scan rate, which is 0.1 V/s. Mn[T(*p*-OH)PP] has an oxidation potential of -0.4525 and -0.9514 V and a reduction potential of -0.3709V, whereas ΔE is equal to -0.0816V (Fig. 2b) and the

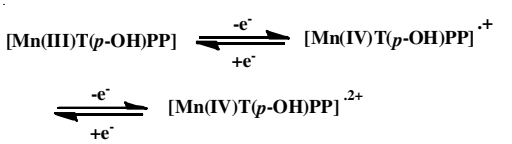

Scheme-I: Plausible oxidation processes of [Mn(III)T(*p*-OH)PP]

$E_{1/2}$ was -0.4117V. The decrease anodic to cathodic peak current ratio for Mn[T(*p*-OH)PP is 1.22. It demonstrates that the growth of the π anion radical caused the quasi-irreversible transfer to take place. The reduction peak appears at -0.3709 V, indicating that Mn(III) to Mn(II) porphyrin is reduced as a result of TBAP's chloride ions, which results in the porphyrin being exceedingly large electron and destabilizing the oxidation state of Mn(II) [19]. The production of Mn(II) ions is shown in **Scheme-II**.

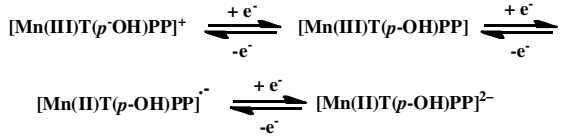

Scheme-II: Plausible reduction processes of [Mn(III)T(*p*-OH)PP]

From Fig. 2c, reduction products have measured at 0.09 V/s scan rate, first and second reduction potentials of porphyrin ligand showed in Fig. 2c. The lowering of anodic to cathodic peak current ratio, i_{pc}/i_{pa} were 1.1 and 1.1, which confirmed two one electrons transfer.

Reduction properties of Mn[T(*p*-OH)PP]: The reduction characteristics of Mn[T(*p*-OH)PP] were determined by utilizing a UV-visible spectrophotometer to detect their reduced products and axial coordination properties. The spectra of Mn[T(*p*-OH)-PP] show the distinctive multiples. Figs. 3-5 depict the development of Soret band and Q band-based Mn(III) *meso*-hydroxy porphyrin complex.

As shown in Fig. 3, Mn[T(*p*-OH)PP] illustrations separated three Soret bands at 395, 413 and 485 nm as a result of the interaction between the Mn orbitals and the porphyrin π* orbital. Comparable to porphyrin (π-π*) transitions are porphyrin (π)-metal (dπ) charge-transfer transitions. When the energies of

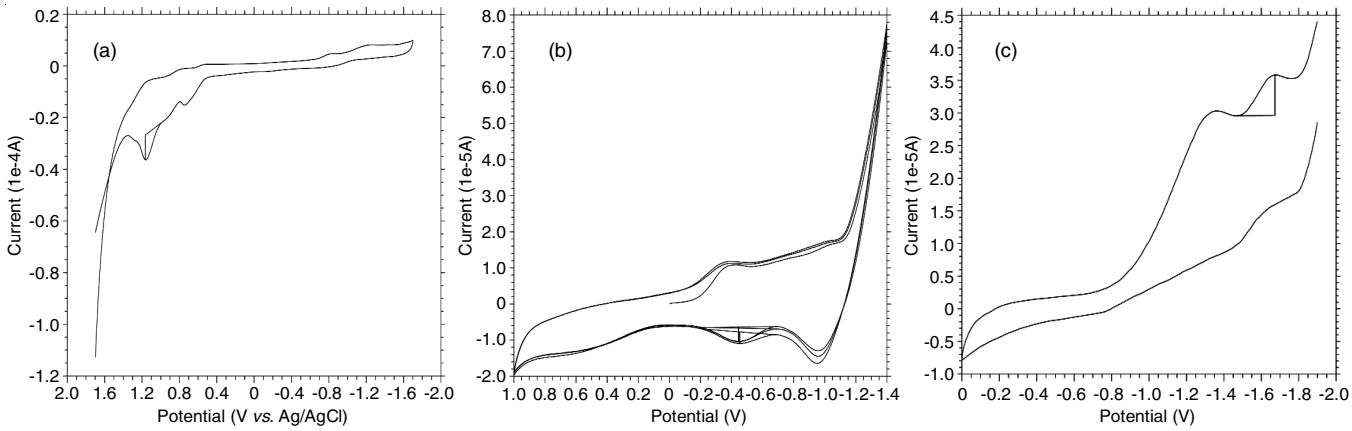

Fig. 2. Cyclic voltammogram of 0.5 × 10^{-3} M Mn[T(*p*-OH)PP] with 0.1 M TBAP recorded in dichloromethane at a room temperature with different scan rates of 0.03 V/s (a), 0.1 V/s (b) and 0.09 V/s

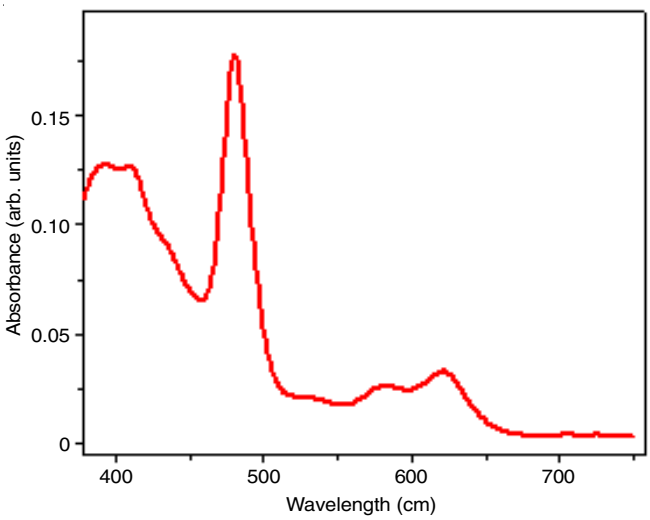

Fig. 3. Visible spectrum of Mn[T(*p*-OH)PP]

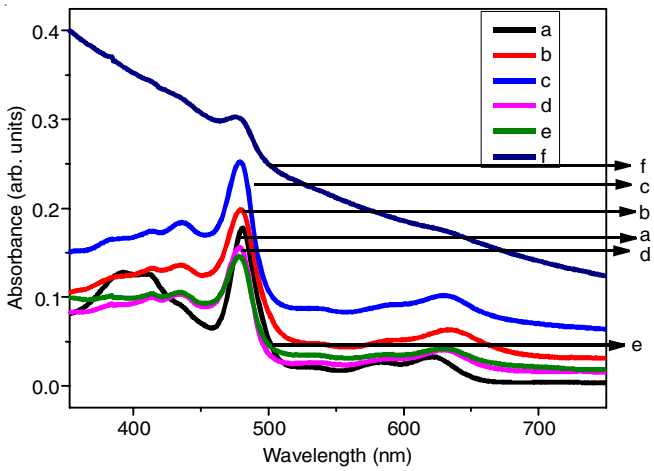

Fig. 4. Reduction characteristics of Mn[T(*p*-OH)PP] with primary amine in dichloromethane found in the visible spectra recorded at room temperature

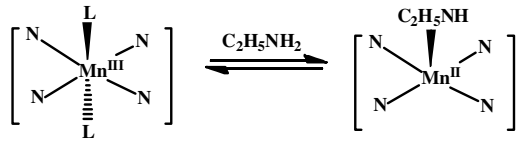

Mn(III) porphyrin
Octahedral geometry

Mn(II) porphyrin
Square pyramidal geometry

Scheme-III: Influence of primary amine on the geometry of Mn(III) *meso* porphyrin

the π-π* and π-d charge transfers are equal, a multiples Soret band is observed. The D_{4h} symmetry of Mn(III) spectrum suggests that it may be a strong metal-porphyrin π interaction. A metal-porphyrin π-contact will occur if Mn atom is on the porphyrin's plane. Because it is an octahedral system with a high spin d^4 spin state, Mn(III) is the strongest interaction between the Mn and the four pyrrole nitrogen donors of porphyrin. A typical Q band can be coupled to the band at 582 nm, which is produced by the ligand transition π-π*. Charge transfer transition π-dπ is considered to be responsible for the band at 625 nm [20,21].

Fig. 4 shows that after increasing the wavelengths of the split soret bands (from 395 to 410 nm and 413 to 434 nm, respectively) two of the split soret bands from Fig. 4 diminish in intensity following the subsequent accumulation of primary amine in Fig. 4e (b, c and d). Hence, only one soret band exists. Finally, it show that Mn(III) porphyrin can be converted to Mn(II) porphyrin by the loss of one electron (**Scheme-III**). A Mn(II) porphyrin with a high spin d^5 configuration is formed, with the primary amine filling the $d_{x^2-y^2}$ orbital at the fifth position. Because of the low orbital energy, Mn(II) is unlikely to be on the porphyrin's plane. Mn(II) porphyrin now has a square pyramidal structure as its form. Fig. 4 depicts Mn(II) porphyrin with primary amine added, which exhibits a typical visible spectrum (b, c, d and e). The fifth position of Mn(II) porphyrin has one amine occupied by π-anion radicals and dianions of Mn as an axial ligand (II). The presence of Q band following reduction and the lack of band widening in the 700-800 nm range are indications of a weakly interacting of metal-ligand approaches through charge-transfer transitions as observed in earlier work [22]. These results imply that increased accumulation (or combinations of mono and dimeric radical types) may be encouraged by hydroxy-substituted porphyrin. By using hydroxyl groups for intermolecular axial coordination and primary amine to provide metal-metal axial bridging contacts, this phenomenon can be rearranged. These findings show that once Mn[T(*p*-OH)PP] aggregates, the shape of Mn[T(*p*-OH)PP] changes from octahedral to square pyramidal [23]. The resultant spectrum specifies a Mn(III)/Mn(II) decrease, per earlier investigations [2]. Reoxidation with $SbCl_5$ resulted in the regeneration of the normal Mn(III) spectra, demonstrating that the product remained steady throughout the investigation. This suggests that the compound switches from Mn^{3+} state, where there is a solid contact between the four pyrrole N and metal, which is relieved by the back donation after metal to ligand, to Mn^{2+} state, where metal-porphyrin π bonding is not preferred and the spectra of Mn(II) are normal.

Electron-donating hydroxy groups increase the red shift of the bands in Mn(III) porphyrins that correspond to the visible spectrum when *p*-substituted porphyrins in the *meso*-position are present. The electrical effect may take two different forms. The axial anion's σ and π interaction with the metal may have two possible effects. The charge of porphyrin could be raised *via* sigma and π donation from the axial ligand to the metal [24]. When the secondary amine of dimethylamine was added repeatedly, a new band at 543 nm develops in Fig. 5b and gradually drops in wavelength from 543 to 540 nm. The band at 540 nm also vanishes in Fig. 5b-d. The transitions are described as a charge transfer from a porphyrin to a manganese metal. If the π-back binding in the tetragonal complexes is weaker, then the charge transfer band should be blue-shifted and the d-level should be decreased. In Fig. 5a-d, the π-π* band bathochromic would move from 385 to 419 nm in this situation, stabilizing the porphyrin e_g^* orbital. Therefore, it would appear that the formation of tetragonal complexes reduces π-bonding. This could happen as a result of the porphyrin's in-plane metal of manganese being widened to accept two axial ligands spaced quite far from the metal of manganese. Fig. 5a,c show two novel Q bonds that occur in the visible spectrum, one at 720 nm and one at 624 nm, respectively. Due to a single spin-allowed

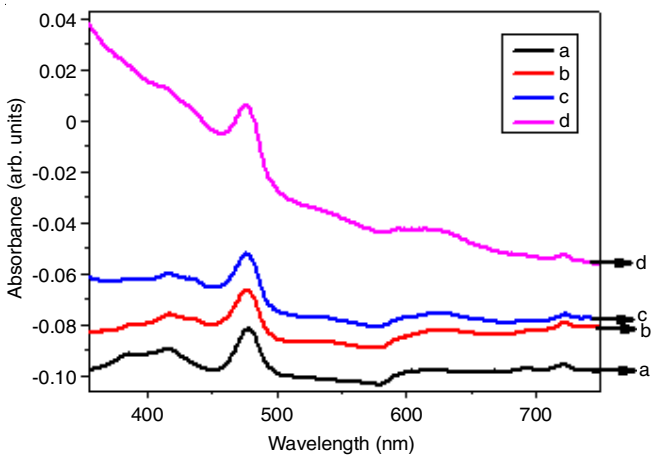

Fig. 5. Reduction characteristics of Mn[T(*p*-OH)PP] with secondary amine in dichloromethane found in the visible spectra recorded at room temperature

transition, Mn(III) porphyrin exhibits a broad strong band at 720 nm that can be attributed to a $^5E_g \rightarrow {}^5T_{2g}$ transition. Jahn-Teller distortion can subject to the Mn^{3+} cation. The distortion converts the coordination site's octahedral to tetragonal (D_{4h}) (**Scheme-IV**) symmetry [18]. The t_{2g} orbital breaks into the e_g and b_{2g} orbitals under the tetragonal distortion, whereas the e_g orbital splits into the a_{1g} and b_{1g} orbitals. As a result, three absorption bands rather than one are seen in a tetragonal site. The e_g orbital is further deformed into the singly degenerate a_{1g} and b_{1g} orbitals [25].

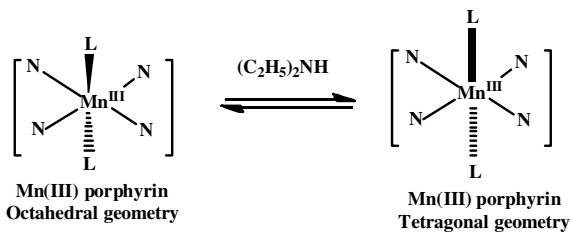

Scheme-IV: Influence of secondary amine on the geometry of Mn(III) *meso*-porphyrin

After the addition of *tert.*-amine, several Soret reductions result in Fig. 6b-e and the production of Mn(II) porphyrin normal spectra in Fig. 6d. At 480 nm, a new band formed, indicating the beginning of polymerization through an π-anion radical. Mn(III) porphyrin undergoes polymerization and transforms into Mn(II) porphyrin by the formation of anion radicals [23].

Oxidation activities of Mn[T(*p*-OH)PP]: The oxidation characteristics of Mn(III) porphyrins have been studied *via* addition 0.5 mM $SbCl_5$ in quartz cuvette. The electronic spectra in Fig. 7 demonstrate the existence of hyper type electronic spectra for Mn(III) *meso*-hydroxy porphyrin with a half vacant metal orbital and symmetry e_g. The charge transfer band of Soret band is the intense band between 400 and 479 nm. The transfer of the porphyrin's a_{1u} (π) and a_{2u} orbitals to Mn e_g orbitals is thought to be the cause of this band. Two bands are observed in the visible region between 539 and 610 nm, whereas the band Q bands are red-shifted [26].

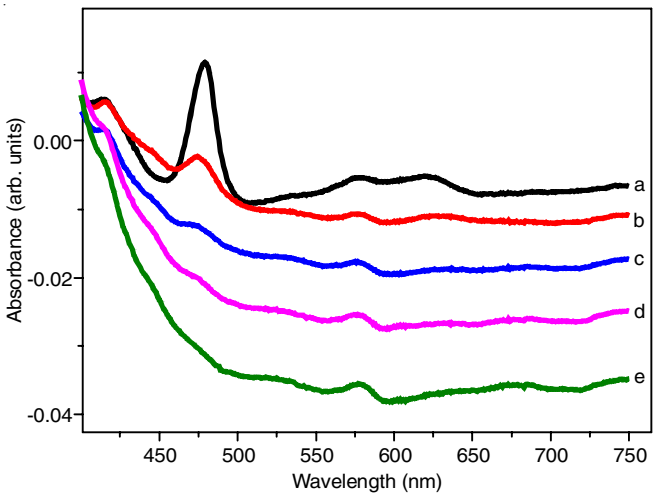

Fig. 6. Reduction characteristics of Mn[T(*p*-OH)PP] with *tertiary* amine in dichloromethane found in the visible spectra recorded at room temperature

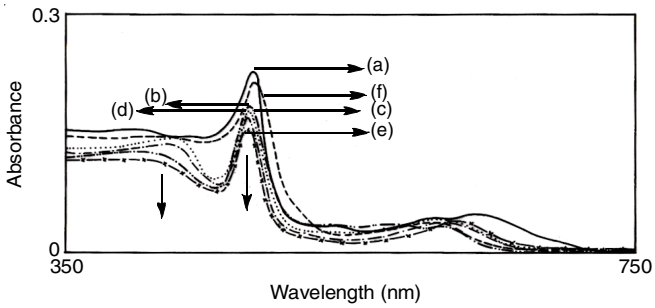

Fig. 7. Absorption spectra of Mn[T(*p*-OH)PP] in CH_2Cl_2 with $SbCl_5$ recorded at ambient temperature

Blue shift and hypochromic shift both cause the band in Mn[T(*p*-OH)PP to shift from 479 to 471 nm and reduce the intensity of the peak. The band at 1.1632 V indicates that a monocation or dication radical may occur. According to the oxidation at 0.9280 V, the bandwidth seen at 634 nm is suggestive of a porphyrin mono-radical cation. The Mn(IV)-porphyrin unit was stabilized by the trianionic ligand (chloride ion obtained from antimony pentachloride) (**Scheme-V**) and changing the geometry from octahedral to distorted pseudo-tetrahedral geometry with approximately C_{3v} symmetry, the oxidation potentials must be shifted higher because the hydroxy group is the electron donating group [18,27].

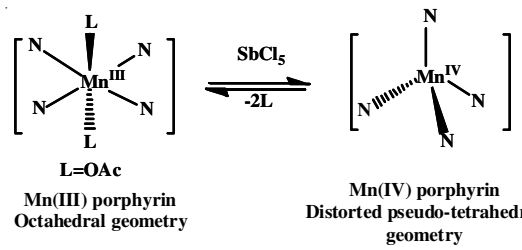

Scheme-V: Influence of $SbCl_5$ on the geometry of Mn(III) *meso*-porphyrin

Conclusion

The UV-visible spectra of Mn(III) hydroxy *meso*-porphyrins show that the geometry of metalloporphyrin compound changes

from octahedral to square pyramidal after the formation of primary amine, which is confirmed by CV data. According to CV data, Mn(III) is oxidized to Mn(IV) porphyrins, which was supported by the porphyrin UV-visible spectrum after its geometry changed to a distorted pseudo-tetrahedral shape. Redox processes have occurred in Mn(III) *meso*-porphyrins, as shown by CV and UV- Vis spectrophotometric measurements.

CONFLICT OF INTEREST

The authors declare that there is no conflict of interests regarding the publication of this article.

REFERENCES

1. S. Lesage, H. Xu and L. Durham, *Hydrol. Sci. J.*, **38**, 343 (1993); https://doi.org/10.1080/02626669309492679
2. P. Tagliatesta, J. Li, M. Autret, E. Van Caemelbecke, A. Villard, F. D'Souza and K.M. Kadish, *Inorg. Chem.*, **35**, 5570 (1996); https://doi.org/10.1021/ic960148c
3. C.-Y. Huang, W.-L. Yeh and S.-H. Cheng, *J. Electroanal. Chem.*, **577**, 179 (2005); https://doi.org/10.1016/j.jelechem.2004.11.029
4. J.R. Irigoyen, L.M. Blanco and S.T. Lopez, *Int. J. Electrochem. Sci.*, **7**, 11246 (2012).
5. A.K. Burrell, W.M. Campbell, D.L. Officer, S.M. Scott, K.C. Gordon and M.R. McDonald, *J. Chem. Soc., Dalton Trans.*, 3349 (1999); https://doi.org/10.1039/a902931a
6. K. Araki, A.L. Araujo, M.M. Toyama, M. Franco, C.M.N. Azevedo, L. Angnes and H.E. Toma, *J. Porphyr. Phthalocyanines*, **2**, 467 (1998); https://doi.org/10.1002/(SICI)1099-1409(199811/12)2:6<467::AID-JPP84>3.0.CO;2-E
7. G.D. Bajju, Deepmala, S.K. Anand, S. Kundan and N. Singh, *Int. J. Electrochem.*, **2013**, 409375 (2013); https://doi.org/10.1155/2013/409375
8. K.D. Borah and J. Bhuyan, *J. Coord. Chem.*, **72**, 2251 (2019); https://doi.org/10.1080/00958972.2019.1654092
9. V. Thandiayyakone, A. Murugan, C.R. Ravikumar, T. Rajkumar, P.T. Arasu, H.S. Yadav and P. Kotteeswaran, *Mater. Today Proc.*, **47**, 933 (2021); https://doi.org/10.1016/j.matpr.2021.04.621
10. J. Ramesh, S. Sujatha and C. Arunkumar, *RSC Adv.*, **6**, 63271 (2016); https://doi.org/10.1039/C6RA09148B
11. A. Murugan, V. Thandiayyakone, S. Kumarasamy, C.R. Ravikumar, S. Muthaiah, M. Chakrabarty, P.T. Arasu, T. Rajkumar and H.S. Yadav, *Asian J. Chem.*, **33**, 26 (2020); https://doi.org/10.14233/ajchem.2021.22905
12. G. Simonneaux, V. Schunemann, C. Morice, L. Carel, L. Toupet, H. Winkler, A.X. Trautwein and F.A. Walker, *J. Am. Chem. Soc.*, **122**, 4366 (2000); https://doi.org/10.1021/ja994190t
13. A. Ghosh, I. Halvorsen, H.J. Nilsen, E. Steene, T. Wondimagegn, R. Lie, E. van Caemelbecke, N. Guo, Z. Ou and K.M. Kadish, *J. Phys. Chem. B*, **105**, 8120 (2001); https://doi.org/10.1021/jp011984x
14. A. Bettelheim, B.A. White, S.A. Raybuck and R.W. Murray, *Inorg. Chem.*, **26**, 1009 (1987); https://doi.org/10.1021/ic00254a011
15. R. Harada, H. Okawa and T. Kojima, *Inorg. Chim. Acta*, **358**, 489 (2005); https://doi.org/10.1016/j.ica.2004.08.009
16. T.A. Evans, G.S. Srivatsa, D.T. Sawyer and T.G. Traylor, *Inorg. Chem.*, **24**, 4733 (1985); https://doi.org/10.1021/ic00220a060
17. M. Liu and Y.O. Su, *J. Electroanal. Chem.*, **426**, 197 (1997); https://doi.org/10.1016/S0022-0728(96)04968-6
18. N.M. Berezina, M.E. Klueva and M.I. Bazanov, *Macroheterocycles*, **10**, 308 (2017); https://doi.org/10.6060/mhc170507b
19. D.P. Goldberg, A.G. Montalban, A.J.P. White, D.J. Williams, A.G.M. Barrett and B.M. Hoffman, *Inorg. Chem.*, **37**, 2873 (1998); https://doi.org/10.1021/ic970624e
20. L.J. Boucher, *J. Am. Chem. Soc.*, **92**, 2725 (1970); https://doi.org/10.1021/ja00712a024
21. F. Tutunea, Dissertations, Spectroelectrochemistry and Voltammetry of Metalloporphinones, Marquette University, Milwaukee, Wisconsin, USA (2011).
22. L.J. Boucher, *J. Am. Chem. Soc.*, **90**, 6640 (1968); https://doi.org/10.1021/ja01026a014
23. A. Murugan, E.R. Nagarajan, A. Manohar, A. Kulandaisamy, A. Lemtur and L. Muthulaksmi, *Int. J. ChemTech Res.*, **5**, 1646 (2013).
24. L.J. Boucher, *Ann. N. Y. Acad. Sci.*, **206(1 The Chemical)**, 409 (1973); https://doi.org/10.1111/j.1749-6632.1973.tb43226.x
25. S.L. Reddy, T. Endo and G.S. Reddy, Eds.: M.A. Farrukh, Electronic (Absorption) Spectra of 3*d*-Transition Metal Complexes; In: Advanced Aspects of Spectroscopy, IntechOpen: London (2012).
26. W. Harhouri, S. Dhifaoui, Z. Denden, T. Roisnel, F. Blanchard and H. Nasri, *Polyhedron*, **130**, 127 (2017); https://doi.org/10.1016/j.poly.2017.04.008
27. V. Thandiayyakone, A. Murugan, C.R. Ravikumar, T. Rajkumar and H.S. Yadav, *Res. J. Chem. Environ.*, **26**, 8 (2022); https://doi.org/10.25303/2606rjce08014